Journal of ELECTRONIC MATERIALS, Vol. 36, No. 4, 2007
DOI: 10.1007/s11664-006-0051-y
© 2007 TMS
Special Issue Paper

Ion Beam Analysis of Amorphous and Nanocrystalline Group III-V Nitride and ZnO Thin Films

J. KENNEDY,[1,2,5] A. MARKWITZ,[1,2] H.J. TRODAHL,[2] B.J. RUCK,[2]
S.M. DURBIN,[3] and W. GAO[4]

1.—National Isotope Centre, GNS Science, Lower Hutt, New Zealand. 2.—The MacDiarmid Institute for Advanced Materials and Nanotechnology, Victoria University of Wellington, Wellington, New Zealand. 3.—Department of Electrical and Computer Engineering, MacDiarmid Institute for Advanced Materials and Nanotechnology, University of Canterbury, Christchurch, New Zealand. 4.—Department of Chemical and Materials Engineering, The University of Auckland, Auckland, New Zealand. 5.—E-mail: j.kennedy@gns.cri.nz

The ion beam analysis (IBA) techniques of Rutherford backscattering spectrometry (RBS), elastic recoil detection analysis (ERDA), nuclear reaction analysis (NRA), and particle-induced x-ray emission (PIXE) have been used to quantitatively determine composition, uniformity, impurity, and elemental depth profiles of major, minor, and trace elements of group III-V nitride and zinc oxide (ZnO) thin films prepared by various growth techniques. The IBA revealed that an amorphous GaN film prepared by ion beam assisted deposition (IBAD) has large variations in film thickness and composition coupled with typically 10–20% oxygen that was found to be essential to stabilize their amorphous structure. The IBA characterization of plasma-assisted molecular beam epitaxy (PAMBE) grown GaN, InN, and InCrN films revealed composition, impurity, and uniformity information of the films. The IBA of ZnO films prepared by radio frequency (RF) sputtering showed that the Zn/O ratio often varied significantly over the film thickness. Hydrogen was found to be a major impurity in the films with around one present in the as-deposited ZnO films. It is clearly shown that the nondestructive, quantitative, and rapid IBA measurements are very useful to develop and optimize growth protocols in respect to film thickness, stoichiometry, and especially in regard to hydrogen and oxygen impurities for group III-V nitride and ZnO thin films prepared by various growth techniques.

Key words: Ion beam analysis (IBA), group III-V nitride thin film, zinc oxide (ZnO), composition

INTRODUCTION

The preparation and characterization of advanced optoelectronic material thin films has attracted tremendous scientific attention in recent years. It is well known that the structural, electrical, and optical properties of thin films are strongly correlated to their composition, microstructure, film thickness, and impurities. For the various applications, an in-depth understanding of the elemental composition at the surface, and in the bulk of the material, is the basis for understanding their properties.

Ion beam analysis (IBA) techniques such as Rutherford backscattering spectrometry (RBS), elastic recoil detection analysis (ERDA), nuclear reaction analysis (NRA), and particle-induced x-ray emission (PIXE) are frequently applied to quantitatively determine composition, uniformity, impurities, and elemental depth profiles of major, minor, and trace elements of advanced material thin films. [1–5]

Over the last few years, our group has been involved in several research projects related to the

(Received August 04, 2006; accepted October 27, 2006; published online January 26, 2007)

production and characterization of various advanced materials. We have used IBA techniques to successfully characterize many advanced material thin films prepared by different conventional techniques: synthesis of thin silicon nitride and oxide films prepared by nitridation and oxidation techniques,[6] stoichiometric and depth profile analysis of Heusler thin films prepared by pulsed laser deposition,[7] multilayered superconducting thin films of Ta_xGe_{1-x} alloys,[8] elemental analysis of prefired and fully reacted superconducting thin films ($Y_1B_2C_3O_{7-x}$) prepared by the inexpensive sol-gel method,[9] and helium ion implantation to create surface–near nanoporous cavity structures in titanium and titanium alloys for biomedical applications and their uptake of light elements such as oxygen.[10]

In the last few years, significant progress has been made in the growth of group III-nitride family (GaN, InN, InGaN, and GaMnN) and zinc oxide (ZnO) semiconductor thin films due to their great importance for various photoelectronic devices such as blue, violet, and near ultraviolet LEDs and laser diodes.[3,11–14] Several groups have started to grow polycrystalline and amorphous GaN and ZnO films using various growth techniques.[15–18]

In this contribution, application of IBA techniques with key results emphasizing the usefulness of IBA for various group III-V nitride and ZnO thin film research and development are presented: (1) compositional and depth profile analysis of amorphous gallium nitride (a-GaN) and GaMnN films prepared by ion beam assisted deposition (IBAD); (2) IBA characterization of plasma-assisted molecular beam epitaxy (PAMBE) grown GaN, InN, and InCrN films; and (3) probing for hydrogen impurities and stoichiometry variations in as-deposited ZnO films prepared by radio frequency (RF) sputtering and PAMBE techniques.

IBA TECHNIQUES

Ion beam analysis comprises a suite of analytical techniques based on ion-matter interactions.[19–22] The techniques use high-energy ion beams of light elements provided by particle accelerators. Typically, MeV (million electron volt) particles hit the surface of a solid-state material. Different ion-matter interactions occur. The incident particles can be (1) scattered in a backward direction (RBS), (2) scattered in the forward direction (ERD), (3) penetrate into the nuclei and cause nuclear reactions (NRA) and particle-induced γ-ray emission, and (4) excite the electron shell (PIXE). In general, all elements of the periodic table can be studied; the analysis techniques are atomically nondestructive, highly sensitive, only a small amount of material is required, and, in many cases, even depth profiles can be measured. For the measurements, solid-state samples are mounted inside a high-vacuum analysis chamber. No specific sample preparation is required for the measurements. The schematic diagram of the typical IBA setup is shown in Fig. 1.

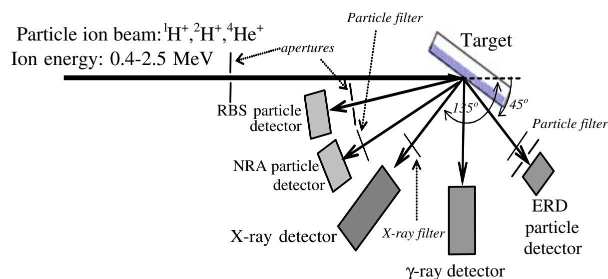

Fig. 1. Typical experimental arrangement for IBA analysis.

Rutherford Backscattering Spectrometry

The RBS is known to be one of the techniques ideal for analysis of thin films.[1,21] An RBS spectrum can be interpreted based on the following key principles: the energy of the elastically scattered beam is proportional to the mass of the target nuclei, the cross section (yield of backscattered particles) is proportional to the elemental composition of the target material, and the incident beam and the backscattered particles loose energy as they pass through the sample. Thus, scattering events that occur at a certain depth occur at a lower energy in the spectrum. Elemental concentrations of matrix components and impurities can be investigated, and the depth profiles of almost every element of the periodic table can be measured.

Elastic Recoil Detection Analysis

The ERDA technique is similar in many aspects to RBS, except that forward scattering is used. In standard geometry, the sample is bombarded with high energy ions (in our case, 2.5 MeV helium) and the recoiled hydrogen atoms are detected with a surface barrier detector (SBD).[4,19] The energy of the detected particles is dependent on the energy transfer occurring during the ion-target atom collision. A thin foil is used in front of the SBD to stop the scattered primary beam from reaching the detector. The ERDA is widely used for advanced material thin films and surfaces to determine mainly hydrogen concentration in the order of a few parts per million.

Nuclear Reaction Analysis

Nuclear reactions induced by bombardment with energetic protons, deuterons, or alpha particles cause the emission of other energetic particles that can be used for elemental analysis.[7] The NRA is best applied to light elements, because nuclear reactions on light nuclei often have large Q values resulting in large yields. Particle selection techniques are straightforward. The SBDs attached with thin film absorbers are commonly used. By consideration of cross sections, Q values, and kinematical properties, it is possible to optimize the working conditions for

different materials. The sensitivity of the technique is very high for light elements.[23] For heavy elements, the Coulomb barrier reduces the cross sections, thereby limiting the applications. Typically, carbon, nitrogen, and oxygen concentrations are measured.

Particle-Induced X-Ray Emission

In PIXE, inner-shell electrons are inelastically scattered by fast moving light particles, such as protons, thus exciting the atom, which then emits characteristic x-rays of the element. The Si(Li) detectors with energy resolution of typically 150 eV are used to detect the characteristic x-rays. These characteristic x-rays help to uniquely identify the presence of the element in the sample.[24]

GROUP III-NITRIDE THIN FILM ANALYSIS

Amorphous GaN Characterization

We have used the IAD technique to deposit amorphous GaN films on silicon, glassy carbon, and quartz substrates.[18,25] It is a vacuum deposition process that combines physical vapor deposition with energetic ion bombardment. Energetic ions impart substantial energy to the film-substrate interface and growing film, ensuring denser, uniform, low-stress, and adherent films. Films were coated in a vacuum system with a base pressure of less than 2×10^{-6} mbar. The details of the film preparation and their structural and optical characterization results are presented in Refs. 18 and 25–28.

The composition of the a-GaN films has been varied by changing the bombardment parameters such as ion-energy and ion-flux in order to optimize the conditions to obtain stochiometric films. The RBS was used to measure our initial film composition. We used a 2.5 MeV $^4He^+$ ion beam impinging on the samples under normal incidence using the 3 MV Van de Graaff accelerator at the Institute of Geological and Nuclear Sciences (Lower Hutt, New Zealand). The SBD detector for measuring the energy of the backscattered particles was mounted at 165°. A low ion current density of 10 nA mm^{-2} was used to measure the samples nondestructively in short time (less than 15 min).[4] Typical RBS spectra obtained on a-GaN films deposited on glassy carbon and silicon substrates are shown in Fig. 2.

The RBS technique detects the number of atoms per unit area in a layer. Using the material density, the film thickness can be calculated in conventional units such as nanometers or micrometers. The energy loss of the ion contains depth information. Therefore, by analyzing the shape of the energy spectrum of the emitted ion yields (counts), information on the concentration profiles can be obtained. Thickness and composition information were extracted from the spectra using the data deconvolution software, Rutherford universal manipulation program (RUMP).[29]

It can be seen from Fig. 2 that nitrogen, carbon, and gallium can be detected and the peaks are interference free, because the substrate material is carbon, which has lower mass than the film elemental masses. Glassy carbon is the ideal substrate for measuring the film thickness, composition, impurity, and depth related information with high accuracy by RBS. The thickness of this particular film was 1.6×10^{18} at. cm^{-2}, which corresponds to 180 ± 5 nm by taking the material density of 6.1 gm^{-3} into account.

It was found that around 20 at.% oxygen is present in these particular films. In addition, an around 50 nm thin surface oxide layer was found in both films, which is linked to oxidation occurring during sample storage in air. Figure 2 also shows that the film is not very smooth and has a roughness of around 20–30 nm. This film is from one of our very first series of GaN films. After this analysis, we changed our deposition parameters such as base pressure and ion energy in order to reduce the level of impurities and to improve the smoothness of the films.

For films deposited onto silicon, it is obvious that the N and O signals are interfered by signals from the silicon substrate. In order to accurately measure the composition and to probe for the depth information of N and O in the films deposited on Si, we have used the NRA technique. Deuteron beams of 920 keV (20–30 nA, 1-mm diameter) were used for the NRA experiments. The particles were detected with a SBD detector (active area of 300 mm^2, Mylar absorber thickness 10.6 μm) mounted at 150°. The nuclear reactions $^{16}O(d,p_1)^{17}O$ ($d\sigma/d\Omega = 4.6$ mb/sr), $^{14}N(d,\alpha_0)^{12}C$ ($d\sigma/d\Omega = 0.1$ mb/sr), and $^{12}C(d,p_0)^{13}C$ ($d\sigma/d\Omega = 55$ mb/sr) were used to determine the concentrations of C, N, and O in the films.[4,9,30] The standard materials of anodically oxidized Ta_2O_5 and TiN were used for calibration purposes. A typical NRA spectrum obtained from an a-GaN film deposited on silicon is plotted in Fig. 3.

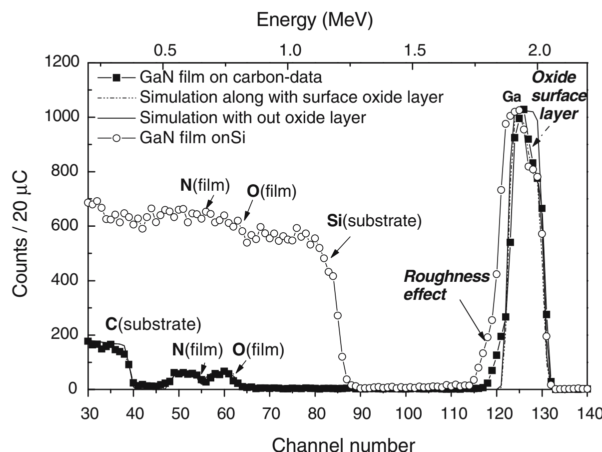

Fig. 2. RBS spectra along with RUMP simulation of a-GaN film deposited on glassy carbon and Si (100).

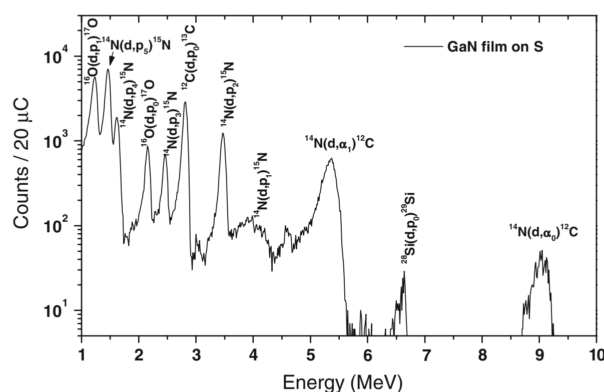

Fig. 3. NRA spectrum from a GaN film deposited on a silicon substrate.

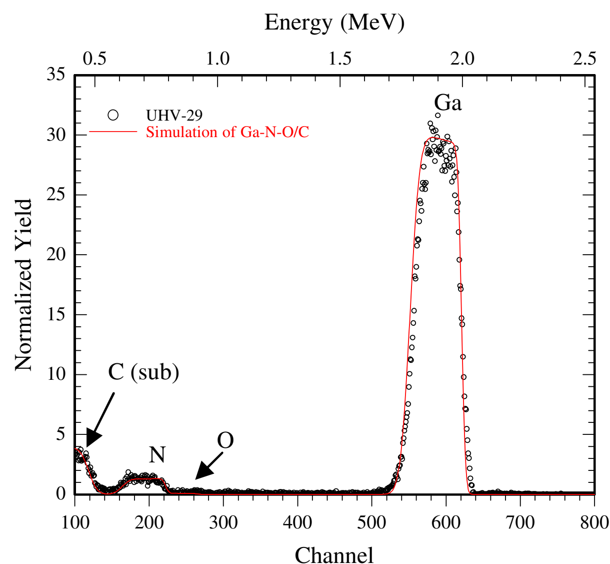

Fig. 4. RBS spectra of an a-GaN film deposited on glassy carbon under UHV conditions.

Figure 3 shows independent peaks for the light elements N and O. Carbon impurities can also be seen. The peak width corresponds to the thickness of the film, and the peak height can be converted to concentration, taking the cross section and stopping power values into account.

The influence of the film thickness on the stoichiometry of a-GaN films was investigated by RBS for films deposited on glassy carbon at ion energy of 500 eV. It was found that the thickness ranges from 100 nm to 270 nm, the variation of Ga/N is within 5–10%, and the Ga/O ratio varies by 10–15%. The concentration of C impurities was 1.0 ± 0.1% in all samples. In order to understand how the concentrations of N and O depend on deposition parameters such as ion energy, measurements were performed on samples deposited at varying ion energy from 40 eV to 900 eV. The Ga/N ratios close to unity were measured for specimens produced in the ion energy region from 400 eV to 700 eV. However, for samples produced at 800 eV and 900 eV ion energy, the Ga/N ratio was measured as 1.3. Additionally, the O concentration is reduced by 5–10% compared to the films deposited at 100–700 eV. The Ga/N atomic ratio is approximately one for films grown with ion energy near 500 eV; these films have the highest transparency. Films grown with ion energies below 300 eV are Ga rich and show reduced transparency across the visible.

Studies of these films with Raman and XRD and optical conductivity measurements established the amorphous nature of the materials.[26,27] The films grown at 500 eV were transparent across the visible region and showed an edge whose energy and structures were in close agreement with crystalline material, suggesting a low density of gap states and homopolar bonds. In addition, structural investigations were carried out on a-GaN with around 10–20% O using x-ray absorption near edge spectroscopy.[28] It was found that around 5–20% of the nitrogen in the films is in the form of molecular N_2 that interacts only weakly with the surrounding matrix. The atomic scale structure of the GaN and the amount of N_2 depend on the growth conditions and the level of oxygen impurities.

In order to reduce the oxygen content in the films, we have deposited a series of films under ultrahigh vacuum (UHV) conditions using 500 eV nitrogen ions. This process was performed in a UHV chamber with a base pressure of ~5×10^{-9} mbar using thermal evaporation of a Ga source and a Kaufmann-type source for the N ions, directed at the substrates, which were Si and glassy carbon. The RBS and NRA measurements were carried out on these films under the experimental conditions described earlier.

Figure 4 shows the RBS spectra along with RUMP simulation for a GaN film deposited on glassy carbon with base pressure of around 5×10^{-9} mbar. It was found that only around 0.5–2% of O is present in the films. X-ray diffraction and x-ray absorption fine structure measurements show that stoichiometric low-oxygen films are composed of nanocrystallites of ~3–4 nm in size and in contrast to GaN films containing up to 20 at.% oxygen, which are amorphous.

In order to incorporate O into UHV films, we have also grown films in an additional partial pressure of ~5×10^{-6} mbar of O, H, or H_2O or grown using a mix of N_2^+ and H_2^+ ions. The RBS, NRA, and ERD measurements were performed on the samples in order to probe for Ga, N, O, and H. The RBS was performed using a 2.5 MeV $^4He^+$ beam. The backscattered particles were detected using SBD places at 165° target-detector angle (active area of 50 mm^2). The samples were analyzed for composition and thickness using the RUMP simulation code.[29]

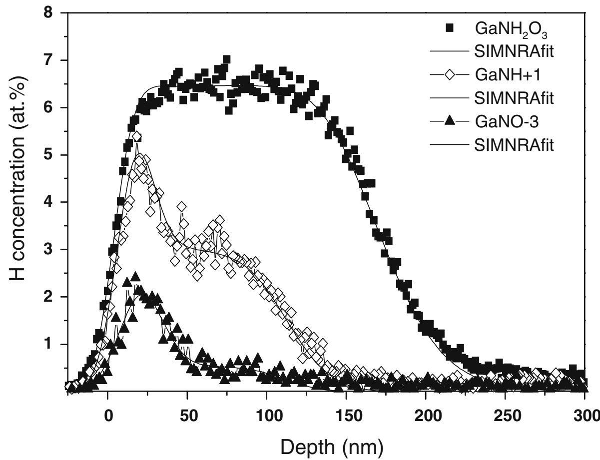

Fig. 5. Hydrogen depth profiles extracted from ERD spectra using SIMNRA.

The ERD analysis technique is widely used to measure hydrogen with a limit of detection of better than 0.1 at.% in many semiconducting films such as SiC and GaN. The ERD measurements were carried out using 2.5 MeV $^4He^+$ ions (beam current of 10 nA and beam diameter of 0.5 mm). The angle of incidence with respect to the target was 20°, and the ERDA detector was placed at 30°. A Mylar film of 10-μm thickness was attached in front of the detectors to stop all the scattered and recoil atoms except hydrogen. The depth resolution was estimated to be better than 50 nm at the surface using the FWHM of the H surface peak from a standard Si wafer. Hydrogen-implanted Si samples were used as calibration standards.

Figure 5 shows H concentration depth profiles extracted from the ERD spectra obtained from a GaN film deposited on Si using SIMNRA.[31] The shape of the ERD spectra indicates homogenous hydrogen distribution throughout the films after taking elastic recoil cross-sectional values, stopping power values, and straggling effects into account. The composition of films grown with a N_2 partial pressure in the chamber varies from a stoichiometric Ga:N ratio to a 10% N excess.

It is observed that molecular N_2 is incorporated into the films, explaining the N excess. The O concentration of these films is less than 1 at.%. The films labeled $GaNH_2O_3$ are grown in differing partial pressures of H_2O. It is found that oxygen can be incorporated to ~13 or ~25 at.% in the films, partially substituting nitrogen. Hydrogen is incorporated into these films as well, in the range of ~5 at.%. Films grown with an O partial pressure or with a mix of N_2^+ and H_2^+ ions are found to incorporate O or H, respectively, but at a much lower concentration (3 at.%) than films grown with an H_2O partial pressure. It is clear that an H_2 partial pressure is not sufficient to incorporate significant amounts of H into the films.

In summary, IBA techniques have been applied successfully to determine the oxygen concentrations and Ga/N ratios, which are used to understand the changes in the structural properties. It is shown that it is not possible to stabilize an amorphous GaN film without incorporating at least 10–15% oxygen. The formation of amorphous GaN films with the introduction of oxygen into the bonding network may be associated with a relaxation of constraints on the bonding network by the presence of nontetrahedral bond configurations centered on oxygen. The GaN films prepared under UHV conditions (low oxygen) possess a nanocrystalline structure with neatly random stacked nanocrystals.[27]

GaMnN and MnN Films Prepared by IAD

Ion beam analysis measurements were carried out to measure the composition and dopant or impurity concentrations in the GaMnN films used for the studies related to realization of a room-temperature ferromagnetic semiconductor.[32,33] We have deposited a series of MnN and Mn doped GaN films using IAD.

Figure 6 shows typical RBS spectra of the MnN and Mn doped GaN films deposited by IAD. From RBS results, it was found that MnN films vary in thickness from 150 nm to 250 nm. Almost stoichiometric Mn/N films were grown for most of the samples. Very little oxygen (less than 1%) was measured in the films. Because Ga and Mn are close in mass, one can see in the GaMnN RBS spectra that it is not possible to separate Ga from Mn peaks, using a 2–3 MeV helium beam.

In order to accurately determine the Mn concentrations, we have performed PIXE measurements at the same time as we have measured the RBS spectra. Figure 7 shows the PIXE spectrum from a typical GaMnN sample. In the PIXE spectra, elements were identified based on their characteristic

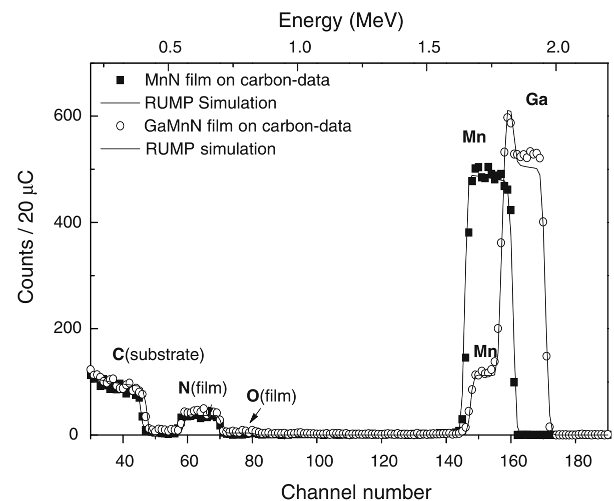

Fig. 6. RBS spectra along with RUMP simulation of MnN and GaMnN films deposited on glassy carbon substrates.

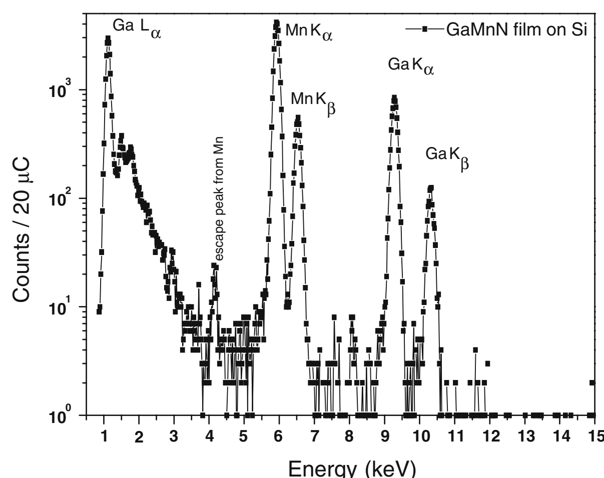

Fig. 7. Typical PIXE spectra from a GaMnN sample deposited on silicon.

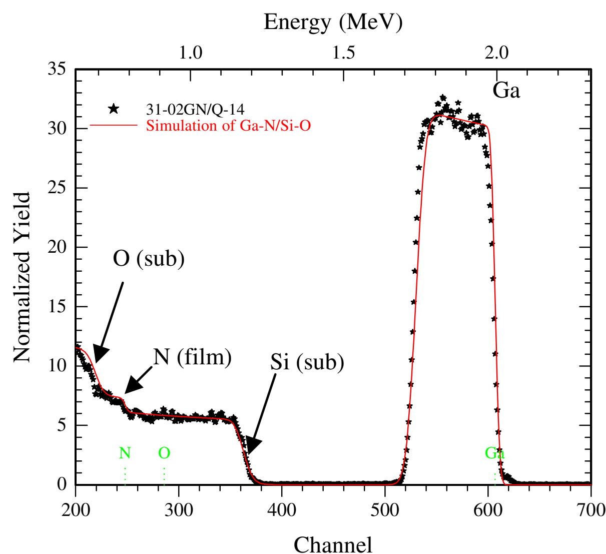

Fig. 8. Typical RBS spectra obtained in GaN films deposited on quartz.

x-ray energy and peak height corresponding to concentration. We have used GUPIXE[34] data deconvolution software to extract the concentration values. It was found that Mn varies between 4% and 12% in our films.

PAMBE Grown Group III-Nitride Film Characterization

A PAMBE technique was employed for growth of heteroepitaxial nitride thin films. The film properties very much depend on their composition and the distribution of matrix elements. In this section, we present the IBA results used to probe for film composition and impurities in GaN, InN, and InCrN films grown on various substrates using the PAMBE system.

We have grown a range of GaN and InN thin films on various substrates (silicon, fused silica glass, sapphire, and glassy carbon) using molecular beam deposition in conjunction with an inductively coupled RF nitrogen plasma source. Indium and Ga elemental fluxes were provided by standard Knudsen 60 cc effusion cells located 30 cm from the substrate and loaded with 7 nines purity metals. Each cell was fitted with a pneumatic shutter that can block the flux if required. Before growth was initiated, the thermal effusion cells were heated to the target temperature and allowed to stabilize for 90 min. Fluxes were measured by a quartz crystal microbalance placed in the substrate position.[35]

In the case of silicon, the surface oxide was removed before deposition. The substrates were then outgassed at 100°C above the substrate temperature during deposition (with a minimum temperature of 650°C). The films were grown at temperatures up to 800°C with a total metal flux in the order of 10^{14} atoms cm^{-2} s^{-1} at a nitrogen pressure of 10^{-5} mbar. These conditions resulted in growth rates between 25 nm h^{-1} and 500 nm h^{-1} and resulted in films grown in either metal-rich or nitrogen-rich growth regimes.

In our first series of GaN films, IBA measurements show gallium rich in stoichiometry. It was also found that at least 10% oxygen was incorporated in all films prepared in this series due to a faulty nitrogen leak valve placed after the nickel filter.[36] After reducing the oxygen contamination, we prepared various GaN films on silica glass and sapphire substrates using different growth conditions in order to optimize stoichiometry and to improve the electrical and optical properties. In all cases, the initial stage of growth appears to proceed as an amorphous film, as indicated by in-situ reflection high-energy electron diffraction (RHEED). A polycrystalline ring pattern emerges within a minute, corresponding to a thickness of several nanometers. This behavior is observed regardless of whether the substrate is heated, although radiative heating leads to a minimum substrate temperature of approximately 60°C.[36]

Figure 8 shows a typical RBS spectrum of a 570 nm ± 10 nm GaN film deposited on a fused silica glass substrate. As can be seen in the figure, the Ga signal is in the background-free region of the RBS spectrum, whereas the nitrogen signal is superimposed with the Si signal from the quartz substrate. The NRA measurements were used to determine the N concentrations. It was found that the Ga/N ratio was determined to 1.12 ± 0.04. No oxygen was detected in the bulk of the films within the sensitivity of the techniques, but all films grown at substrate temperatures above 200°C were found to be gallium rich. This is somewhat surprising, because increasing the gallium cell temperature from 895°C to 940°C resulted in films with enhanced growth rate, implying growth occurs under gallium-limited conditions in the present setup. Adjusting the RF power supplied to the

plasma source and varying the nitrogen flow rate had no discernable effect on film stoichiometry. Surprisingly, three films grown below 200°C were found to be slightly nitrogen rich in content. Because the cracking efficiency of the plasma source is rather low (approximately 2%), there is considerable molecular nitrogen present during growth.[37] Whether the enhanced nitrogen content is due to a reduction of antisite defects or molecular nitrogen (e.g., split interstitials) is still under investigation.

The RBS and NRA measurements were carried out on films prepared with different growth temperature on quartz substrate. It was found that films grown at low temperature (150°C) are slightly N rich compared to films grown at higher temperatures (500–650°C). In all cases, films grown on silica glass substrates were found to be polycrystalline and largely c-axis oriented.

In order to probe the uniformity and thickness of the film on 75-mm glass wafer, which was used to deposit the GaN film, we have performed RBS and NRA measurements at various places. Figure 9 shows the depth profile extracted using RUMP. It was found that the Ga concentration did not change significantly. However, the thickness changed from 700 nm to 950 nm. Note we have used the density of crystalline GaN of 6.1 gm^{-3} to obtain a depth scale. It was also found that a native oxide layer of around 80 nm exists for these films, which might be caused by the films being exposed to air for many days.

As discussed in the "Amorphous GaN Characterization" section, various nuclear reactions from N, O, and Si can be measured simultaneously via NRA. Note that the interference-free peak for nitrogen is measured via the (d,α) reaction $^{14}N(d,\alpha_0)^{12}C$. Figure 10 shows NRA spectra measured at various different spots of the same GaN film. One can see that there is no difference in the peak height in the spectra, which is an indication for a uniform GaN film regarding the nitrogen concentration. However,

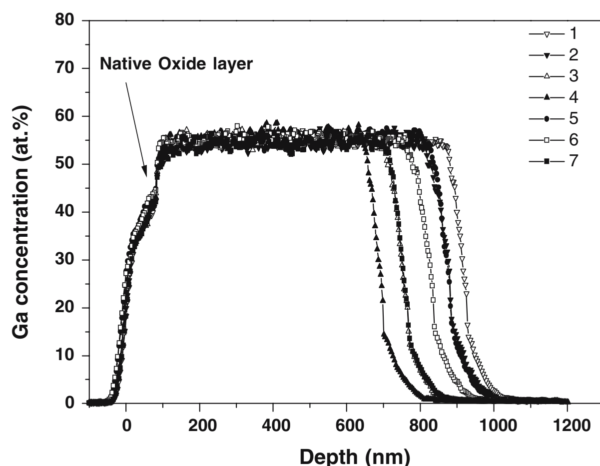

Fig. 9. Gallium depth profiles of GaN films deposited on glass extracted from RBS.

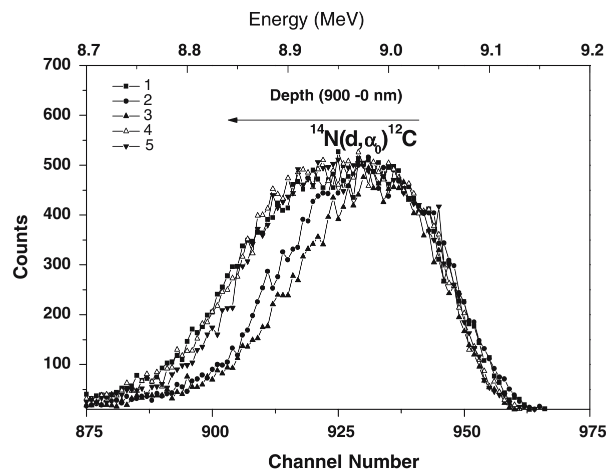

Fig. 10. NRA spectra of a GaN film deposited on silicon substrate measured at various different positions on the target *via* the $^{14}N(d,\alpha_0)$ ^{12}C reaction.

the peak width varies, which is a measure for thickness variations. This is in agreement with the RBS results.

Single crystalline and polycrystalline indium nitride films have been grown on (0001) sapphire and fused silica glass using PAMBE.[38] The IBA measurements revealed the existence of a thin layer (~50 nm) of indium oxynitride at the surface of all InN films investigated, which have a stoichiometric In/N ratio and are oxygen free (oxygen concentration < 0.1 at.%).[39]

InCrN Film Characterization

In recent years, wide bandgap semiconductors have been identified as being the most promising materials for achieving high Curie temperatures. Among several candidates based on group III nitrides for spintronics applications, InCrN is a very interesting material because of the two binary end points of the InCrN alloy, diamagnetic InN and antiferromagnetic CrN.[40]

We have deposited several series of InCrN film on (0001) sapphire. Active nitrogen was supplied by an Oxford Applied Research HD25 RF plasma source operating at 1.25 SCCM and 250 W. Indium, Ga, and Cr were supplied by effusion cells with fluxes of approximately 10^{14} $cm^{-2}s^{-1}$. For the InCrN growth, around 150 nm of GaN buffer layer was deposited at 650°C followed by InCrN at 450 °C. The details of the growth parameters are described in Ref. 41.

Figure 11 shows a typical RBS spectrum obtained for an InCrN film deposited on sapphire using a 2.5 MeV helium beam. It can be seen that the Cr surface peak at channel number 150 (energy = 1.75 MeV) is superimposed by the In signal. In addition, the Ga signal from the GaN buffer layer also appears in the spectra around channel 115. From the RBS results, we have determined the In and Ga concentrations. The NRA was used at the

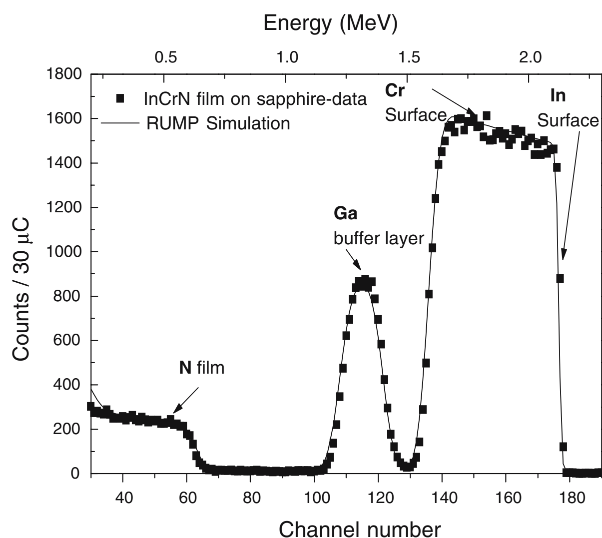

Fig. 11. RBS spectrum along with RUMP simulation of an InCrN film deposited on sapphire.

same time to determine the N concentration in the films.

The PIXE was applied to determine the Mn content in GaMnAs films prepared by MBE.[13] In order to measure Cr concentrations below 10 at.%, PIXE measurements were conducted along with RBS using the same incident ion beam. Figure 11 shows the PIXE spectra obtained for three different InCrN films deposited under different deposition conditions. It can be seen from the PIXE spectrum that the Cr peaks (K_α and K_β) vary in height in the three samples. The Cr concentration was calculated using GUPIX. It was found that our InCrN films contain between 0.5% and 4% Cr.

In addition, one can also see the In and Ga peaks from the films and the Al peak from the sapphire substrate. Note that a reference InN film is also plotted in Fig. 12 to confirm the presence of Cr in the InCrN films. The inset in Fig. 12 shows PIXE spectra of a representative InCrN film and InN reference, around the Cr K_α peak region for comparison purposes. Unlike XRD, which can only estimate the Cr content through the assumption that Vegard's law holds, the PIXE result indicates the total Cr in the film. Coupled with XRD, we were able to determine that further increasing the Cr content in an effort to improve magnetic properties led to increased Cr interstitials as opposed to substitutional incorporation.

ZNO FILM CHARACTERIZATION

Zinc oxide is promising for various technological applications especially optoelectronic, short wavelength light emitting devices due to its wide, direct band gap. One of the advantages of ZnO over other currently used wide band gap semiconductors such as GaN is its nearly 3 times higher exciton binding energy (60 meV), in comparison to others such as ZnSe (22 meV) or GaN (25 meV). It also provides optically efficient excitonic behavior up to or even above room temperature.[42,43] ZnO is stable at elevated temperature and therefore it can withstand high-temperature annealing and treatment processes associated with doping and forming of ohmic contacts. It is expected that degradation due to the generation of defects during operation will not pose a serious problem for ZnO based materials.

It is well known that the electrical and optical properties of ZnO are strongly correlated to the composition and stoichiometry of the sample,[44–46] so that accurate determination of these remains an important issue. Numerous fabrication techniques have been implemented in the growth of ZnO thin films on various substrates, including metal-organic

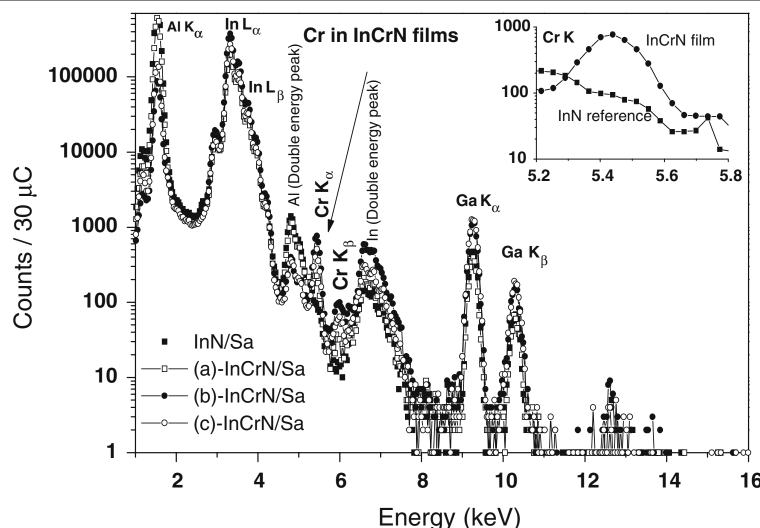

Fig. 12. PIXE spectra of three different InCrN films deposited on sapphire. An InN on sapphire films is measured for reference. The inset shows the presence of Cr in the InCrN film.

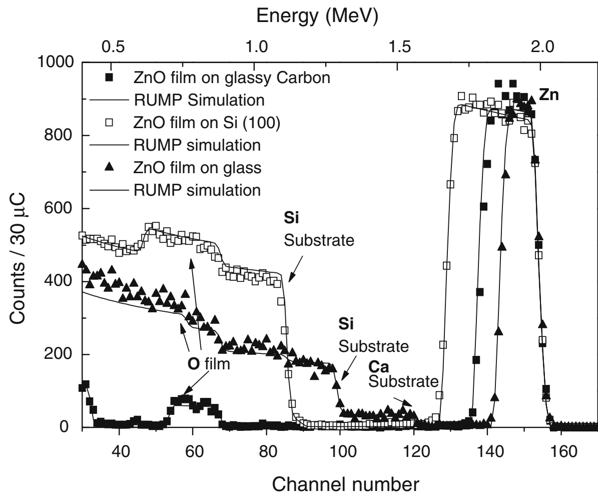

Fig. 13. RBS spectra along with RUMP simulations of three ZnO films deposited on glassy carbon, silicon, and glass substrates.

chemical vapor deposition, sol-gel deposition, DC or RF magnetron sputtering, reactive evaporation, spray pyrolysis, and pulsed laser deposition, each of which might be expected to exhibit different stoichiometry tendencies as well as background impurities and defects.[47–50]

Recently, we have started to deposit series of ZnO films on various substrates using the RF/DC magnetron sputtering technique and RF-PAMBE. The IBA techniques have been used to determine the composition and impurity in the films in order to optimize the deposition parameters to obtain improved electrical and optical properties of ZnO film.

RF Sputtered ZnO Film Characterization

We have deposited a range of ZnO thin films on silicon (100), quartz, glass, and glassy carbon substrates using RF magnetron sputtering under the best optimized deposition parameters described in Ref. 50. Before loading the substrates into the vacuum chamber, the substrates were ultrasonically cleaned in acetone, rinsed with alcohol, and then dried in hot air. The sputtering was performed with an rf power 250 W. The details of the sample preparation are described in Ref. 50. The glassy carbon substrates were used only for ion beam analysis purposes.

The RBS data were obtained using a 2.5 MeV $^4He^+$ beam with a current of 20–30 nA. The samples were mounted on the computer-controlled stepping motor stage and a collimated (1.5-mm slit type) surface barrier detector was positioned at a scattering angle of 165°. The solid angle of the RBS experimental arrangement was 0.075 msr. Figure 13 shows the RBS spectra obtained from three ZnO films deposited on three different substrates loaded at the same time in the RF sputter system. Different mounting positions of the substrates in the deposition chamber amount for different film thicknesses (refer to the Zn signal for example). RUMP[29] simulations were used to extract the thickness and concentration of films. The film thickness in the glassy carbon substrate is 2.1×10^{18} at. cm^{-2}, which is around 250 nm by taking into account a ZnO density of 5.6 g cm^{-3}, in the silicon substrate 3.2×10^{18} at. cm^{-2} (thickness = 380 nm), and in the glass substrate 1.5×10^{18} at. cm^{-2} (thickness = 180 nm).

We have also investigated the variations of film composition for the films deposited on different substrates. The composition of the film remains the same. It was found that all of the films are slightly Zn rich (Zn/O ratio of 1.01), which is common for ZnO films. ZnO always deviated from stoichiometry and present intrinsic defects such as Zn interstitials and O vacancies. Note, some films from other series were measured to be significantly overstoichiometric (Zn/O > 1.0) for all substrates.

Structural and optical measurements were carried out by XRD, SEM, and PL. A strong (002) preferential orientation was measured for the ZnO films deposited on the three different substrates irrespective of thickness. This indicates polycrystallinity with hexagonal structure and preferential orientation along the *c*-axis. This is due to the lowest surface free energy of the (002) plane in ZnO.[51] These results suggest that the grains grow along the (002) direction. The SEM results of all the films show homogenous distribution of grains that are smaller for the Si substrate compared to the glass and quartz substrates, which are possibly due to the smoothness of the silicon wafer.

Photoluminescence properties were studied on the films deposited on all three substrates with various thicknesses. On the film of thickness over 250 nm deposited on silicon, a sharp emission peak was observed around 380 nm corresponding to UV near band edge emission and a broad peak from 450–650 nm in green light emission.[50] The Hall effect measurements were carried out in all samples in order to measure the charge carrier. All of our films show an n-type carrier concentration ranging from 3×10^{15} to 3×10^{18} /cm^3, mobility of 6–50 cm^2/V·s, and resistivity of 0.02–100 ohm·cm.

In general, ZnO exhibits strong n-type conductivity because of intrinsic donor defects such as oxygen vacancies (V_O) or Zn interstitials (Zn_I), which are formed during the deposition procedure. However, recent first-principle calculations revealed that none of the native defects can provide a high concentration of shallow donors and that hydrogen impurities might be responsible for n-type conductivity.[52] Therefore, it will be useful to determine the concentration of hydrogen in the ZnO films. Figure 14 shows a typical ERD spectrum of a ZnO film deposited on Si measured with a 2.5 MeV helium beam.

Figure 14 shows the typical surface H contamination from channel 390–340, which is a typical feature of solid-state surfaces. The hydrogen concentration of the ZnO film was extracted by

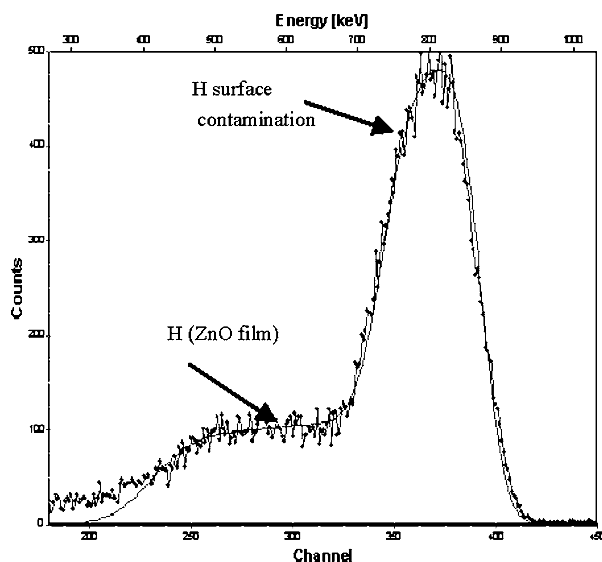

Fig. 14. ERD spectrum and SIMNRA simulation of a ZnO film deposited on Si; specimen surface at channel 390, surface peak channels 390–340, and film/substrate interface around channel 230.

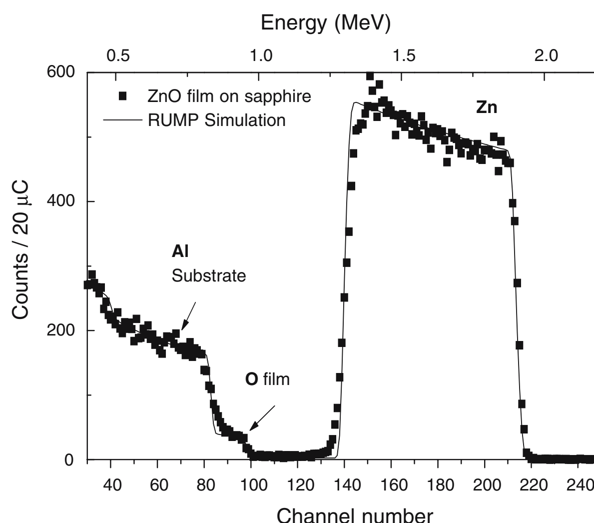

Fig. 15. RBS spectrum and RUMP simulation of a ZnO film deposited on sapphire by PAMBE.

SIMNRA.[31] It was found that around 1% ± 0.1 hydrogen was present in the film deposited on Si, whereas around 3–4 ± 0.1% was present on the films deposited on glass and quartz substrates,[53] which might be due to the enhanced surface roughness of the glass and quartz substrates that increases the surface area increasing the probability of absorption of hydrogen during deposition.

PAMBE Grown ZnO Film Characterization

ZnO thin films were deposited onto *c*-plane sapphire substrates using a modified Perkin-Elmer 430 MBE system with a base pressure of ~1×10^{-10} Torr. The Zn fluxes ranging from 2×10^{13} to 1×10^{15} were provided by evaporating 6 N purity Zn metal in a 60 cc effusion cell. Active oxygen was provided with oxygen gas excited by an Oxford Applied Research MDP21 plasma source, with applied RF power of 300 W. Epiready substrates were mounted onto molybdenum growth blocks using indium bonding.

In the first series of films, the oxygen flux was kept constant while the Zn flux was varied to try to observe the dependence of stoichiometry of the samples on the Zn:O flux ratio. The RBS measurements were carried out using the similar condition described in our earlier section. A typical RBS spectrum and RUMP[29] simulation are plotted in Fig. 15. It was found that the stoichiometry can range widely from excessively oxygen rich (Zn:O < 1) to excessively Zn rich (Zn:O > 1). There appears to be no significant correlation between the applied Zn flux and the measured stoichiometry.[54]

A second series of samples were grown directly on sapphire with a growth temperature of 550°C. Again, the Zn flux was varied while all other parameters were kept constant to investigate the effect of the changing Zn:O flux ratio. It was found that there is no observable correlation between the stoichiometry and the growth temperature. Further, the crystalline quality was studied by RBS and channeling. The minimum yield of the ZnO peak under the channeling condition is around 10%, which indicates good crystalline quality of the single crystals, consistent with the photoluminescence characterization performed separately.[54]

SUMMARY

As we have illustrated by several examples, ion beam analysis techniques can be very useful in the successful development of deposition protocols of various growth techniques for thin films such as GaN, GaMnN, InCrN, and ZnO. Compositional and depth profile analyses were performed on *a*-GaN and GaMnN films prepared by IBAD. The IBAD has enabled us to probe for impurities of O and H in the films and to optimize the thickness and deposition parameters. The IBA characterization of PAMBE grown GaN, InN, and InCrN films revealed composition and uniformity of the films and, in particular, allowed for low concentration determination of Cr in this potential spintronics material. Regarding ZnO films deposited under the same conditions, it was observed that the Zn/O stoichiometry is independent of the substrate material used. The ERD revealed that hydrogen impurities were incorporated to different concentrations into the films during the preparation process. In summary, the above investigations highlight the usefulness of IBA as a key analytical tool for research and development of advanced materials.

ACKNOWLEDGEMENTS

The authors thank the GNS Science (formerly the Institute of Geological & Nuclear Sciences) IBA team members and our collaborators from the Victoria University of Wellington, the University of Canterbury, and the University of Auckland for their significant contributions to the work discussed in this paper. This project is supported by the Foundation for Research Science and Technology of New Zealand.

REFERENCES

1. J.P. Stoqurt and T. Szorenyi, *Phys. Rev. B* 66, 144108 (2002).
2. S. Pereira, M.R. Correia, E. Pereira, K.P. O'Donnell, C. Trager-Cowan, F. Sweeney, and E. Alves, *Phys. Rev. B* 64, 205311 (2001).
3. Y. Kang and D.C. Ingram, *J. Appl. Phys.* 93, 3954 (2003).
4. V.J. Kennedy, A. Markwitz, U.D. Lanke, A. McIvor, H.J. Trodahl, and A. Bittar, *Nucl. Instrum. Meth.* B190, 620 (2002).
5. A. Markwitz, V.J. Kennedy, S.M. Durbin, P.B. Johnson, A. Mucklich, and N. Dytlewski, *Surf. Interface Analysis* 36, 317 (2004).
6. A. Markwitz and G.V. White, *Adv. Mater.* 13, 1027 (2001).
7. C. Grigorescu, E. Valerio, L. Tortet, R. Notonier, H.J. Trodahl Kennedy V.J., A. Markwitz, S.A. Manea, and M. Autric, *J. Cryst. Growth* 275, e1183 (2005).
8. A. Engel, H.J. Trodahl, A. Markwitz, and V.J. Kennedy, *Mod. Phys. Lett. B* 15, 1314 (2001).
9. V.J. Kennedy, A. Markwitz, A. Bubendorfer, N. Long, and N. Dytlewski, *Curr. Appl. Phys.* 4, 292 (2004).
10. P.B. Johnson, A. Markwitz, and P.W. Gilberd, *Adv. Mater.* 13, 997 (2001).
11. N.M. Johnson, A.V. Nurmikko, and S.P. DenBaars, *Phys. Today* 53, 31 (2000).
12. S. Nakamura and G. Fasol *The Blue Laser Diode*(Berlin, Springer, 1998).
13. K.M. Yu, W. Walukiewicz, T. Wojtowicz, I. Kuryliszyn, X. Liu, Y. Sasaki, and J.K. Furdyna, *Phys. Rev. B* 65, 201303 (2002).
14. D.P. Norton, Y.W. Heo, M.P. Ivil, S.J. Pearton, M.F. Chisholm, and T. Steiner, *Mater. Today* 34, (2004).
15. K. Iwata, H. Asahi, K. Asami, R. Kuroriwa, and S. Gonda, *Jpn. J. Appl. Phys.* 36, L661 (1997).
16. M. Park, J.P. Maria, J.J. Cuomo, Y.C. Chang, J.F. Muth, R.M. Kolbas, R.J. Nemanich, E. Carlson, and J. Bumgarner, *Appl. Phys. Lett.* 81, 1797 (2002).
17. Y. Yang, H. Ma, C. Xue, H. Zhuang, X. Hao, J. Ma, and S. Teng, *Appl. Surf. Sci.* 193, 254 (2002).
18. A. Bittar, H.J. Trodahl, N.T. Kemp, and A. Markwitz, *Appl. Phys. Lett.* 78, 619 (2001).
19. J.R. Tesmer and M. Nastasi*Handbook for Modern Ion Beam Analysis*(Pittsburgh, PA: Materials Research Society,1995).
20. J.R. Bird and J.S. Williams(1989) *Ion Beams for Material Analysis* Academic Press, Australia.
21. W.K. Chu, J.W. Mayer, andM.A. Nicolet*Backscattering Spectrometry* (New York: Academic Press, Inc., 1978).
22. A.F. Morral, P.R. Cabarrocas, and C. Clerc, *Phys. Rev. B* 69, 125307 (2004).
23. V.J. Kennedy, A. Markwitz, G.V. White, and I.W.M. Brown, *Mod. Phys. Lett. B* 15, 1332 (2001).
24. S.A.E. Johansson and J.L. Campbell(1995) *Particle Induced X-ray Emission Spectrometry* Wiley, New York, .
25. U.D. Lanke, et al. , *Mater. Res. Soc. Symp. Proc.* 693, I6 (2002)–101.
26. H.J. Trodahl, F. Budde, B.J. Ruck, S. Granville, A. Koo, and A. Bittar, *J. Appl. Phys.* 97, 084309 (2005).
27. F. Budde, et al. , *J. Appl. Phys.* 98, 063514 (2005).
28. B.J. Ruck, A. Koo, U.D. Lanke, F. Budde, S. Granville, H.J. Trodahl, A. Bittar, V.J. Kennedy, and A. Markwitz, *Phys. Rev. B* 70, 235202 (2004).
29. L.R. Doolittle, *Nucl. Instrum. Meth.* B9, 3341985 (1985).
30. P.B. Johnson, V.J. Kennedy, A. Markwitz, and C. Varoy, *Nucl. Instrum. Meth.* B206, 1056 (2003).
31. M. Mayer *SIMNRA Users Guide*, Report IPP 9/113. (Garching, Germany: Max-Planck-Institute fur Plasmaphysik, 1997) .
32. Y. Cui and L. Li, *Appl. Phys. Lett.* 80, 4139 (2002).
33. B.K. Rao and P. Jena, *Phys. Rev. Lett.* 89, 185504 (2002).
34. J.A. Maxwell, W.J. Teesdale, and J.L. Cambell, *Nucl. Instrum. Meth. B* 95, 407 (1995).
35. V.A. Christie, S.I. Liem, R. Reeves, V.J. Kennedy, A. Markwitz, and S.M. Durbin, *Curr. Appl. Phys.* 4, 225 (2004).
36. V.J. Kennedy, A. Markwitz, R.J. Kinsey, S.M. Durbin, and N. Dytlewski, Proc. 13th Nuclear Techniques of Analysis & 8th Vacuum Society of Australia Congr., p. 151.
37. N. Materer, R.S. Goodman, and S.R. Leone, *J. Appl. Phys.* 83, 1917 (1998).
38. P.A. Anderson, C.E. Kendrick, T.E. Lee, W. Diehl, R.J. Reeves, V.J. Kennedy, A. Markwitz, R.J. Kinsey, and S.M. Durbin, *Proc. SPIE Int. Soc. Opt. Eng.* 90, 5277 (2004).
39. S.M. Durbin, P.A. Anderson, A. Markwitz, and J. Kennedy, *Thin Sold Films* (in press).
40. L.M. Corliss, N. Elliot, and J.M. Hastings. *Phys. Rev*. 117, (1960).
41. P.A. Anderson, R.J. Kinsey, S.M. Durbin, A. Markwitz, J. Kennedy, A. Asadov, W. Gao, and R.J. Reeves, *J. Appl. Phys.* 98, 043903 (2005).
42. D.C. Look, *Mater. Sci. Eng. B* 80, 383 (2001).
43. H.M. Huang, S. Mao, H. Feick, H. Yan, Y. Wu, H. Kind, E. Weber, R. Russo, and P. Yang, *Sci.* 292, 1897 (2001).
44. H.J. Ko, T. Yao, Y.F. Chen, and S.K. Hong, *J. Appl. Phys.* 92, 4354 (2002).
45. H. Kato, M. Sano, K. Miyamoto, and T. Yao, *Jpn. J. Appl. Phys.* 42, 2241 (2003).
46. T. Minami, H. Sato, H. Nanto, and S. Takata, *Jpn. J. Appl. Phys. Part 2* 24, L781 (1985).
47. W. Wernas, A. Yamada, and M. Kawasaki, *Jpn. J. Appl. Phys.* 33, L283 (1994).
48. A. Dutta and S. Basu, *Mater. Chem. Phys.* 34, 41 (1993).
49. X.L. Guo, H. Tabata, and T. Kawai, *J. Cryst. Growth.* 223, 135 (2001).
50. W. Gao and Z. Li, *Ceram. Int.* 30, 1155 (2004).
51. X.L. Xu, S.P. Lau, and J.S Chen, *Mater. Sci. Semicond. Process* 4, 617 (2001).
52. C.G Van de Walle, *Phys. Rev. Lett.* 85, 1012 (2000).
53. J. Kennedy, A. Markwitz, Z. Li, W. Gao, S. Durbin, and R. Reeves (Paper presented at Proc. 4th Int. Conf. on Advanced Materials and Performance (ADMP05), New Zealand, July 11–13, 2005).
54. W.C.T. Lee, J. Kennedy, A. Markwitz, R.J. Kinsey, and S.M. Durbin (Paper presented at Proc. 14th AINSE Conf. on Nuclear and Complementary Techniques of Analysis & 9th Vacuum Society of Australia Congr., Wellington, New Zealand, Nov. 20–22, 2005).